Elastic fields, dipole tensors, and interaction between self-interstitial atom defects in bcc transition metals

S. L. Dudarev* and Pui-Wai Ma†

Culham Centre for Fusion Energy, UK Atomic Energy Authority, Abingdon, Oxfordshire OX14 3DB, United Kingdom

(Received 30 September 2017; published 8 March 2018)

Density functional theory (DFT) calculations show that self-interstitial atom (SIA) defects in nonmagnetic body-centered-cubic (bcc) metals adopt strongly anisotropic configurations, elongated in the ⟨111⟩ direction [S. Han *et al.*, Phys. Rev. B **66**, 220101 (2002); D. Nguyen-Manh *et al.*, *ibid.* **73**, 020101 (2006); P. M. Derlet *et al.*, *ibid.* **76**, 054107 (2007); S. L. Dudarev, Annu. Rev. Mater. Res. **43**, 35 (2013)]. Elastic distortions, associated with such anisotropic atomic structures, appear similar to distortions around small prismatic dislocation loops, although the extent of this similarity has never been quantified. We derive analytical formulas for the dipole tensors of SIA defects, which show that, in addition to the prismatic dislocation looplike character, the elastic field of a SIA defect also has a significant isotropic dilatation component. Using empirical potentials and DFT calculations, we parametrize dipole tensors of ⟨111⟩ defects for all the nonmagnetic bcc transition metals. This enables a quantitative evaluation of the energy of elastic interaction between the defects, which also shows that in a periodic three-dimensional simple cubic arrangement of crowdions, long-range elastic interactions between a defect and all its images favor a ⟨111⟩ orientation of the defect.

DOI: 10.1103/PhysRevMaterials.2.033602

I. INTRODUCTION

Strongly anisotropic self-interstitial defect configurations form spontaneously in body-centered-cubic metals such as sodium [1] or tungsten [2–5] if an extra atom, identical to the atoms of the host material, is inserted in the crystal lattice and the resulting structure is relaxed into the lowest energy configuration. Such anisotropic "crowdion" or "dumbbell" defects are produced simultaneously with vacancies as Frenkel pairs in high-energy collision cascade events [6,7]. The defects have a recognizable anisotropic lattice strain associated with them, illustrated in Fig. 1. The figure shows a self-interstitial defect in tungsten, where the positions of atoms were derived from a density functional theory (DFT) calculation.

Properties of self-interstitial atom (SIA) defects are significantly different from those of vacancies. For example, diffusion of vacancies is thermally activated and observed only at relatively high temperatures, above 650 K in tungsten [8], whereas in the same material the SIA crowdion defects are mobile at temperatures that are as low as several degrees Kelvin [9,10].

The equilibrium structure [3–5] and modes of Brownian motion (diffusion) [10–13] of individual SIA defects in body-centered transition metals are now well-established. Yet, there is still no regular approach to the treatment of evolution of ensembles of such defects, including the effect of elastic interaction between the defects. The difficulty appears fundamental, illustrating the lack of a sufficiently general formalism linking the discrete atomistic representation of structure of nanoscale defects with continuum elasticity.

Recently, we have derived tractable analytical expressions [14] for the energy of elastic interaction between two dislocation loops, and between a dislocation loop and a dilatation center, for example a vacancy cluster. These equations use the notion of an elastic dipole tensor of a dislocation loop, expressed in terms of its Burgers vector, its area, and the unit normal vector to the habit plane of the loop. However, the analysis is based entirely on the treatment of dislocations in elastic continuum, and it cannot be applied to point defects.

Here we aim to explore defects that are too small to be treated using the notions of macroscopic elasticity [15]. Whereas it is in principle possible to describe elastic fields of nanoscale defects using dipole tensors computed numerically [16–20], in practice it is sometimes not convenient, as numerical calculations have to be repeated every time when a defect changes its configuration. For example, this occurs frequently when a SIA defect migrates, as it alters the direction of its motion [4,16]. The effect of applied strain on SIA defects in α-Fe was explored using DFT recently in Ref. [17]. Below, we show how to parametrize the dipole tensor of a defect using certain invariant quantities, for example its elastic relaxation volume, as opposed to dynamic variables that may evolve as functions of time. Dynamic parameters here are the coordinates of the defect [12,13] or the unit vector characterizing the anisotropy of its structure.

We start by deriving an analytical expression for the dipole tensor of a dislocation loop, and then considering the limit of an infinitesimally small loop size. Surprisingly, we find that this seemingly natural approach results in a prediction for the dipole tensor of a point defect that does not agree with numerical calculations even for defects in tungsten, a material that is well described by isotropic elasticity theory. We then derive an analytical representation for the dipole tensor of a defect using a two-parameter tensorial form, which shows that in addition

*sergei.dudarev@ukaea.uk
†leo.ma@ukaea.uk

to a pure prismatic dislocation loop character, the elastic field of a SIA defect also contains a significant *isotropic* dilatation component. We also derive an analytical expression for the energy of interaction between two SIA defects and between a SIA defect and a dilatation center, for example a vacancy cluster.

To illustrate applications of the new formalism, we evaluate the energy of interaction between SIA defects ordered in the form of a periodic superlattice encountered in a DFT calculation. Surprisingly, we discover that the energy minimum of such periodic configuration corresponds to an orientation of the directional unit vector of the defect pointing in a ⟨111⟩ direction.

The analysis given below highlights the part that the notion of elastic fields of point defects plays in the multiscale treatment of microstructural evolution of materials exposed to a flux of high-energy particles. On the one hand, point defects are the elementary building blocks of dislocations and vacancy clusters forming under irradiation. On the other hand, the structure and properties of elementary point defects are strongly influenced by the discreteness of the lattice, making an elasticity-based treatment, which highlights similarities and differences between defects and dislocations, critical to the development of lattice-continuum multiscale models.

II. ELASTIC DIPOLE TENSOR OF A DISLOCATION LOOP AND A SIA DEFECT

The energy of interaction between a defect and external homogeneous strain field $\epsilon_{ij}^{\rm ext}$, according to Eq. (4.99) of Ref. [18], is

$$E = -P_{ij}\epsilon_{ij}^{\rm ext}. \tag{1}$$

Here P_{ij} is the elastic dipole tensor of the defect, and $\epsilon_{ji}^{\rm ext}$ is a slowly varying function of spatial coordinates. Another application of elastic dipole tensors is in a calculation of the energy of elastic interaction between any two defects a and b, given by

$$E_{\rm int}^{ab} = P_{ij}^{a} P_{kl}^{b} \frac{\partial}{\partial x_j}\frac{\partial}{\partial x_l} G_{ik}(\mathbf{r}), \tag{2}$$

where P_{ij}^{a} and P_{ij}^{b} are the dipole tensors of the two defects, $\mathbf{r} = \mathbf{r}_a - \mathbf{r}_b$ is a vector from defect b to a, and x_i are the Cartesian components of $\mathbf{r}$. Equations (1) and (2) are consistent with the fact that elastic strain far from a defect situated at the origin equals

$$\epsilon_{ij}(\mathbf{r}) = -P_{kl}\frac{\partial}{\partial x_j}\frac{\partial}{\partial x_l} G_{ik}(\mathbf{r}). \tag{3}$$

The Green's function of elasticity equations $G_{ik}(\mathbf{r})$ in the isotropic elasticity approximation has the form [21]

$$G_{ik}(\mathbf{r}) = \frac{1}{16\pi\mu(1-\nu)r}\left[(3-4\nu)\delta_{ik} + \frac{x_i x_k}{r^2}\right], \tag{4}$$

where μ is the shear modulus and ν is the Poisson ratio.

In the limit in which the external strain field is homogeneous and independent of spatial coordinates, Eq. (1) can be applied not only to a small defect but also to a dislocation loop of arbitrary size. In this limit, the dipole tensor of a dislocation loop can be found by comparing (1) with Eq. (4–41) of Ref. [15], namely

$$E = -\int b_i \sigma_{ij}^{\rm ext} dA_j, \tag{5}$$

where $\mathbf{b}$ is the Burgers vector of the loop, $\sigma_{ij}^{\rm ext}$ is the stress tensor of the external elastic field, and integration over dA_j is performed over an arbitrary surface bounding the loop. Using Hooke's law,

$$\sigma_{ij} = C_{ijkl}\epsilon_{kl}, \tag{6}$$

and combining Eqs. (5) and (1), we arrive at [14,22,23]

$$P_{ij} = C_{ijkl} b_k A_l, \tag{7}$$

where A_l is a Cartesian component of the vector area $\mathbf{A}$ of the loop, which may be conveniently expressed as a contour integral over the perimeter of the loop as [24]

$$\mathbf{A} = \frac{1}{2}\oint (\mathbf{r} \times d\mathbf{l}). \tag{8}$$

In the isotropic elasticity approximation, where

$$C_{ijkl} = \mu\frac{2\nu}{1-2\nu}\delta_{ij}\delta_{kl} + \mu(\delta_{ik}\delta_{jl} + \delta_{il}\delta_{kj}), \tag{9}$$

the elastic dipole tensor of a dislocation loop acquires the form [14,22]

$$P_{ij} = \mu\left[(b_i A_j + A_i b_j) + \frac{2\nu}{1-2\nu}(\boldsymbol{b}\cdot\boldsymbol{A})\delta_{ij}\right]. \tag{10}$$

The elastic relaxation volume $\Omega_{\rm rel}$, which is a quantity characterizing the degree of macroscopic expansion or contraction (swelling) of the material due to the presence of a defect in it, in the isotropic elasticity approximation under *traction-free boundary conditions*, equals

$$\Omega_{\rm rel} = \frac{(1-2\nu)}{2\mu(1+\nu)}{\rm Tr}\, P_{ij}. \tag{11}$$

Substituting (10) into (11), we find the relaxation volume of a dislocation loop [14,22,23]

$$\Omega_{\rm rel} = (\mathbf{b}\cdot\mathbf{A}) = \frac{1}{2}\oint \mathbf{b}\cdot(\mathbf{r}\times d\mathbf{l}), \tag{12}$$

where the contour integration is performed along the dislocation line forming the perimeter of the loop.

Since the relaxation volume of a self-interstitial prismatic dislocation loop is a positive quantity whereas the relaxation volume of a vacancy loop is negative, Eq. (12) implies that the Burgers vector $\mathbf{b}$ of a prismatic self-interstitial dislocation loop points in the same direction as the surface area vector $\mathbf{A}$. There are two conventions in the academic literature defining the direction of the Burgers vector, which differ in the sign of $\mathbf{b}$; see, for example, Figs. 1–22 by Hirth and Lothe [15] and Fig. 24 by Landau and Lifshitz [24]. This unfortunate inconsistency in the definition of the sign of the most fundamental notion of dislocation theory affects all the equations that contain odd powers of $\mathbf{b}$, including the formula for the relaxation volume of a dislocation loop above. The definition of the relaxation volume of a self-interstitial loop as a positive quantity appears to imply that here we follow the definition by Landau and Lifshitz; see Eq. (27.1) of Ref. [24]. Still, many of the equations

given below are consistent with the results by Hirth and Lothe [15].

The above equation for the relaxation volume remains valid even if the material is elastically anisotropic. In the anisotropic elasticity approximation, the elastic relaxation volume of a defect is given by the trace of a tensor product [18],

$$\Omega_{\rm rel} = S_{kkij} P_{ij}, \tag{13}$$

where $\hat{S} = \hat{C}^{-1}$ is the tensor of elastic compliance [25]. Formula (12) for the relaxation volume of a dislocation loop then follows from the substitution of (7) into (13).

The relaxation volume of a dislocation loop (12) does not depend on elastic properties or the position of the loop in the material. It is a purely geometric property of the dislocation line forming the loop. In particular, the relaxation volume does not depend on the distance between the dislocation loop and the surface, and Eq. (12) remains valid irrespective of the shape of the crystal, provided that the traction-free boundary conditions are satisfied.

It is also useful to derive an expression for the rate of variation of the relaxation volume of a dislocation loop as a function of time. The derivative of the relaxation volume of the loop is [this formula can be derived from Eq. (12) or by differentiating Eq. (4–2) of Hirth and Lothe [15] with respect to time]

$$\frac{d\Omega_{\rm rel}}{dt} = \oint \mathbf{v} \cdot (d\mathbf{l} \times \mathbf{b}) = \oint \mathbf{b} \cdot (\mathbf{v} \times d\mathbf{l}), \tag{14}$$

where $\mathbf{v}$ is the velocity of a dislocation segment $d\mathbf{l}$ at the loop perimeter. If a dislocation loop evolves through self-climb [26] or undergoes thermally activated stochastic glide in the direction of its Burgers vector [27,28,46], the relaxation volume remains constant and $d\Omega_{\rm rel}/dt = 0$. On the other hand, under the conditions of vacancy-mediated climb, the rate of variation of relaxation volume can be positive or negative, depending on the vacancy or self-interstitial nature of the loop [29].

The elastic field of an isotropic point defect, for example a vacancy, is characterized by only one parameter, namely the elastic relaxation volume. The elastic dipole tensor of an isotropic point defect can be written as

$$P_{ij} = \frac{\Omega_{\rm rel}}{3} C_{ijkl} \delta_{kl}. \tag{15}$$

In a cubic crystal this can be simplified further. Using the Voigt notations [25], from (15) we find

$$P_{ij} = \frac{\Omega_{\rm rel}}{3} (C_{11} + 2C_{12}) \delta_{ij}, \tag{16}$$

which in the isotropic elasticity limit, where $C_{11} = 2\mu(1-\nu)/(1-2\nu)$ and $C_{12} = 2\mu\nu/(1-2\nu)$, becomes [14]

$$P_{ij} = \frac{2\mu\Omega_{\rm rel}}{3} \frac{1+\nu}{1-2\nu} \delta_{ij}. \tag{17}$$

To describe a linear anisotropic defect structure, such as the SIA defect shown in Fig. 1, we define a vector $\mathbf{n}$ characterizing the orientation of the axis of the defect, and we write

$$P_{ij} = C_{ijkl} \left(\Omega^{(1)} n_k n_l + \frac{\Omega^{(2)}}{3} \delta_{kl} \right). \tag{18}$$

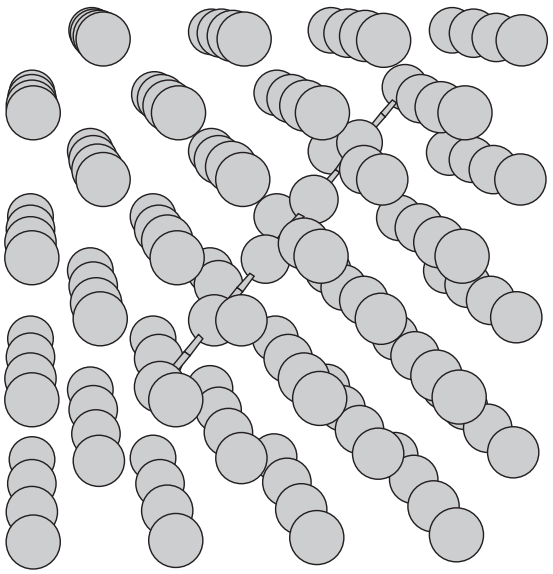

FIG. 1. Atomic structure of a self-interstitial atom defect in tungsten, where the orientation of the axis of the defect is close to the [111] direction. Atomic bonds are shown for the atoms that are significantly closer to each other than atoms in a perfect lattice.

The above expression is a generalization of (7) and (15) to the case in which the structure of the defect is characterized by a unit vector $\mathbf{n}$, out of which we construct a symmetric two-index tensor $n_k n_l$, entering the expression for the dipole tensor analogously to how the Kronecker symbol δ_{kl} enters Eq. (15).

Substituting (18) into (13), we see that the total relaxation volume of a point defect is

$$\Omega_{\rm rel} = \Omega^{(1)} + \Omega^{(2)}. \tag{19}$$

The two parameters $\Omega^{(1)}$ and $\Omega^{(2)}$ are measures of the relative weight of anisotropic and isotropic components of the elastic field of a defect. In the isotropic elasticity limit, where tensor C_{ijkl} is given by Eq. (9), formula (18) becomes

$$P_{ij} = 2\mu\Omega^{(1)} n_i n_j + 2\mu \left[\frac{\nu}{1-2\nu} \Omega^{(1)} + \frac{1}{3} \left(\frac{1+\nu}{1-2\nu} \right) \Omega^{(2)} \right] \delta_{ij}. \tag{20}$$

It is instructive to compare Eq. (20) for the elastic dipole tensor of a SIA defect, and Eq. (10) for the elastic dipole tensor of a dislocation loop. In the pure prismatic loop limit, where the Burgers vector of the loop $\mathbf{b}$ is collinear with the loop area vector $\mathbf{A}$, Eq. (10) can be written as

$$P_{ij} = 2\mu b A \left[n_i n_j + \frac{\nu}{1-2\nu} \delta_{ij} \right]. \tag{21}$$

Here, unit vector $\mathbf{n}$ defines the direction of both $\mathbf{b}$ *and* $\mathbf{A}$. While the similarity between (21) and (20) is apparent, there is also a fundamental difference between the two cases. The dipole tensor of a pure prismatic dislocation loop (21) is fully defined by a single parameter, the product bA, which in this case is the relaxation volume of the loop. On the other hand, defining the elastic dipole tensor (18) of a SIA defect requires two parameters, where parameter $\Omega^{(2)}$ describes the dilatation

component of the elastic field of the defect, absent in the case of a pure prismatic dislocation loop. Numerical calculations of elastic dipole tensors of point defects in various bcc transition metals summarized in the next section show that the dilatation component of elastic fields of defects is non-negligible, suggesting that a SIA defect is an entity fundamentally dissimilar from an infinitesimally small dislocation loop.

III. DENSITY FUNCTIONAL THEORY EVALUATION OF ELASTIC DIPOLE TENSORS

The dipole tensor of a defect can be computed using DFT calculations, or empirical interatomic potentials, by evaluating the response of a simulation cell to external applied strain, namely [30,31]

$$P_{ij} = V_{\rm cell}\left(C_{ijkl}\epsilon_{kl}^{\rm app} - \overline{\sigma}_{ij}\right). \tag{22}$$

Here $V_{\rm cell}$ is the volume of the simulation cell, $\epsilon_{ij}^{\rm app}$ is the external applied strain, and $\overline{\sigma}_{ij}$ is the average homogeneous macroscopic stress associated with the simulation box. Note that the right-hand side of (22) vanishes in accordance with Hooke's law if the cell contains no defect.

To rationalize formula (22), we note that the elastic strain energy of a defect in an infinite medium is given by the volume integral

$$E_D = \frac{1}{2}\int_V \sigma_{ij}\epsilon_{ij}dV, \tag{23}$$

$$= \frac{1}{2}\int_V C_{ijkl}\epsilon_{kl}\epsilon_{ij}dV, \tag{24}$$

where integration is performed over the entire space. In the presence of infinitesimal external strain $\epsilon_{ij}^{\rm ext}$, E_D can be written in the linear approximation in $\epsilon_{ij}^{\rm ext}$ as

$$E_D\left(\epsilon_{ij}^{\rm ext}\right) = E_D\left(\epsilon_{ij}^{\rm ext}=0\right) + \left(\frac{\delta E_D}{\delta\epsilon_{ij}^{\rm ext}}\right)_{\epsilon_{ij}^{\rm ext}=0}\epsilon_{ij}^{\rm ext}. \tag{25}$$

Comparing this with Eq. (1), we find

$$P_{ij} = -\left(\frac{\delta E_D}{\delta\epsilon_{ij}^{\rm ext}}\right)_{\epsilon_{ij}^{\rm ext}=0} \tag{26}$$

$$= -\int_V C_{ijkl}\epsilon_{kl}^D dV = -\int_V \sigma_{ij}^D dV, \tag{27}$$

where ϵ_{ij}^D is the strain and σ_{ij}^D is the stress resulting from the presence of a defect in an infinite medium. The dipole tensor equals the negative of the volume integral of stress induced by the defect.

Numerical simulations often involve the use of periodic boundary conditions. In effect, the use of periodic boundary conditions amounts to simulating an infinite number of defects, each occupying a volume element equivalent to the volume of the simulation cell. The dipole tensor can be computed from the macrostress $\overline{\sigma}_{ij}$ associated with the simulation cell, namely

$$P_{ij} = -\int_{V_{\rm cell}} \sigma_{ij}dV = -V_{\rm cell}\overline{\sigma}_{ij}. \tag{28}$$

Equations (27) and (28) are equivalent in the linear elasticity approximation. This can be proven as follows.

Assume that N identical defects are distributed in an infinite medium. In the limit $N\to\infty$, the total stress is the same as the total stress induced by a defect plus its periodic images,

$$N\int_V \sigma_{ij}^D dV = \int_V \sigma_{ij}^D dV + \sum_n \int_V \sigma_{ij}^{I,n} dV, \tag{29}$$

where $\sigma_{ij}^{I,n}$ is the stress induced by the nth periodic image of the defect. Dividing both sides of the above equation by N, we find

$$\int_V \sigma_{ij}^D dV = \frac{1}{N}\int_V \left(\sigma_{ij}^D + \sum_n \sigma_{ij}^{I,n}\right)dV, \tag{30}$$

$$= \int_{V_{\rm cell}} \sigma_{ij}dV. \tag{31}$$

This is because stress in a simulation cell is equivalent to stress in any periodically translated cell, and the stress within the cell is a linear sum of stresses induced by the defect and all its images.

Concluding this section, we would like to direct the interested reader to several recent publications [32–34], where a number of fundamental aspects of the dipole tensor formalism are explored in considerable detail.

IV. NUMERICAL RESULTS

To evaluate elastic dipole tensors, we performed *ab initio* simulations of the most stable SIA defect configurations in vanadium, niobium, tantalum, molybdenum, and tungsten. In all the nonmagnetic bcc transition metals, the ⟨111⟩ dumbbell configuration has the lowest formation energy in comparison to other SIA defect configurations [4].

Ab initio calculations were performed using the Vienna Ab initio Simulation Package (VASP) [35–38] and the AM05 [39–41] exchange-correlation functional. The plane-wave energy cutoff was 450 eV. To investigate the cell size effect, we performed simulations using simulation cells of different size. For simulation cells containing $4\times4\times4$ bcc unit cells, we used $5\times5\times5$ k-points. In simulations involving $4\times4\times5$ bcc unit cells, we used a $5\times5\times4$ k-point mesh.

First, perfect lattice simulation cells, containing 128 or 160 atoms, were fully relaxed. Then, we created cells containing 129 or 161 atoms, with a SIA defect in a ⟨111⟩ dumbbell configuration. Atomic positions were then relaxed, but the cell size and shape were kept the same as in the perfect lattice case. Elastic dipole tensors for all the metals were computed from macrostresses, using Eq. (28). Results are given in Table I.

We have also computed defect dipole tensors using Eq. (22). Simulation cells containing a ⟨111⟩ dumbbell were fully relaxed, leading to vanishing macrostresses $\overline{\sigma_{ij}}=0$. Simulation cell size is now different from the perfect lattice case, and the deformation of the cell is the same as that resulting from the application of external strain. Numerical results are summarized in Table II. Elastic constants C_{ijkl} were evaluated following the method proposed by Le Page and Saxe [42], using a two-atom cell with $30\times30\times30$ k-points. Values of elastic constants are given in Table III in Voigt notations.

The convergence of *ab initio* results has been verified using molecular statics calculations performed for tungsten

TABLE I. Elastic dipole tensors of ⟨111⟩ SIA dumbbell configurations in W, Mo, Nb, Ta, and V, illustrated in Fig. 2. Dipole tensors were computed using *ab initio* simulations with no volume or shape relaxation of the simulation cells. Matrix elements P_{ij} are given in eV.

129 atoms	P_{11}	P_{22}	P_{33}	P_{12}	P_{23}	P_{31}
W	53.84	53.84	53.84	13.23	13.23	13.23
Mo	40.37	40.37	40.37	7.814	7.814	7.814
Ta	34.68	34.68	34.68	6.645	6.645	6.645
Nb	31.69	31.69	31.69	3.001	3.001	3.001
V	21.28	21.28	21.28	−0.162	−0.162	−0.162
161 atoms	P_{11}	P_{22}	P_{33}	P_{12}	P_{23}	P_{31}
W	52.97	52.97	54.78	12.73	13.07	13.07
Mo	39.60	39.60	41.29	7.213	7.758	7.758
Ta	34.61	34.61	34.22	6.081	6.152	6.152
Nb	32.00	32.00	31.77	2.099	2.023	2.023
V	16.93	16.93	17.47	0.154	−0.132	−0.132

(see Fig. 2). Calculations were performed using LAMMPS [43] and the interatomic tungsten potential (EAM4) developed by Marinica *et al.* [44]. We have followed a procedure similar to that outlined above. First, we have relaxed a number of perfect lattice simulation cells containing various numbers of atoms. Then, we produced an SIA defect in a ⟨111⟩ dumbbell configuration, and we relaxed the atomic positions without relaxing the simulation cell itself. Results are summarized in Table IV. Values of elastic constants characterizing the chosen interatomic potential are given in Ref. [44]. They are $C_{11} = 523$ GPa, $C_{12} = 202$ GPa, and $C_{44} = 161$ GPa. The equilibrium lattice parameter for the EAM4 potential is 3.143 39 Å. Results given in the table show that achieving full convergence requires using relatively large simulation cells, exceeding approximately by a factor of 2 the dimensions presently accessible to a DFT calculation. Still, even with relatively small simulation cells, it is possible to compute the elements of dipole tensors at approximately ∼5% accuracy, sufficient for applications. This assessment of accuracy is confirmed by the analysis of solutions of the Frenkel-Kontorova model for the ⟨111⟩ defects given in [47] and illustrated in Fig. 3.

V. ELASTIC FIELDS AND INTERACTIONS INVOLVING SELF-INTERSTITIAL ATOM DEFECTS

The energy of elastic interaction between two defects with elastic dipole tensors P^a_{ij} and P^b_{kl} in the isotropic elasticity approximation is given by Eq. (2), where the second derivative

TABLE II. Elastic dipole tensors of ⟨111⟩ SIA dumbbell configurations in W, Mo, Nb, Ta, and V. Dipole tensors were computed using *ab initio* simulations with full relaxation of the simulation cells. Matrix elements P_{ij} are given in eV.

129 atoms	P_{11}	P_{22}	P_{33}	P_{12}	P_{23}	P_{31}
W	53.75	53.75	53.75	13.39	13.39	13.39
Mo	40.35	40.35	40.35	7.709	7.709	7.709
Ta	34.37	34.37	34.37	6.069	6.069	6.069
Nb	31.15	31.15	31.15	2.027	2.027	2.027
V	18.13	18.13	18.13	−0.179	−0.179	−0.179

TABLE III. Lattice parameters (in angstroms) and elastic constants (in GPa) of W, Mo, Nb, Ta, and V, evaluated following the method by Le Page and Saxe [42], using a two-atom cell and $30 \times 30 \times 30$ k-points.

	a_0	C_{11}	C_{12}	C_{44}
W	3.149	569.73	211.52	157.16
Mo	3.124	505.43	175.26	108.04
Ta	3.278	293.44	168.18	82.08
Nb	3.282	273.54	143.06	23.62
V	2.956	308.53	147.96	31.31

of the elastic Green's function (4) is

$$\frac{\partial}{\partial x_j}\frac{\partial}{\partial x_l}G_{ik}(\mathbf{r}) = \frac{1}{16\pi\mu(1-\nu)r^3}[(3-4\nu)\delta_{ik}(3\eta_l\eta_j-\delta_{lj}) + 15\eta_i\eta_j\eta_k\eta_l - 3(\delta_{ij}\eta_k\eta_l + \delta_{il}\eta_j\eta_k + \delta_{jl}\eta_i\eta_k + \delta_{kj}\eta_i\eta_l + \delta_{kl}\eta_i\eta_j) + (\delta_{il}\delta_{kj}+\delta_{ij}\delta_{kl})]. \quad (32)$$

In the above equation, η_i is a component of the radial unit vector $\boldsymbol{\eta} = \mathbf{r}/r$. Using expression (20) for the elastic dipole tensors of interacting defects, from (2) we find

$$E_{\rm int} = \frac{\mu(\Omega^{(1)})^2}{4\pi(1-\nu)r^3}[-12\nu(\boldsymbol{\eta}\cdot\mathbf{e})(\boldsymbol{\eta}\cdot\mathbf{n})(\mathbf{e}\cdot\mathbf{n}) + 2(2\nu-1)(\mathbf{e}\cdot\mathbf{n})^2 + 15(\boldsymbol{\eta}\cdot\mathbf{e})^2(\boldsymbol{\eta}\cdot\mathbf{n})^2 + 1 - 3(\boldsymbol{\eta}\cdot\mathbf{e})^2 - 3(\boldsymbol{\eta}\cdot\mathbf{n})^2] + \frac{\mu}{2\pi(1-\nu)r^3}\Omega^{(1)}\left[\nu\Omega^{(1)} + \frac{(1+\nu)}{3}\Omega^{(2)}\right] \times \{[3(\boldsymbol{\eta}\cdot\mathbf{e})^2-1] + [3(\boldsymbol{\eta}\cdot\mathbf{n})^2-1]\}, \quad (33)$$

where vectors $\mathbf{n}$ and $\mathbf{e}$ define orientations of the axes of the two interacting anisotropic SIA defects. Note that the above expression for the energy is quadratic in $\mathbf{n}$ and $\mathbf{e}$ and hence the choice of the specific direction of either of the two vectors is immaterial. It is sufficient to define the orientation of the axes of the defects and the relative position of defects to compute the energy of elastic interaction between them.

If the unit vectors of the two defects are collinear, $\mathbf{n}\|\mathbf{e}$, formula (33) acquires a simple form,

$$E_{\rm int} = \frac{\mu(\Omega^{(1)})^2}{4\pi(1-\nu)r^3}[15(\boldsymbol{\eta}\cdot\mathbf{n})^4 - 6(\boldsymbol{\eta}\cdot\mathbf{n})^2 - 1] + \frac{\mu\Omega^{(1)}\Omega^{(2)}}{3\pi r^3}\frac{(1+\nu)}{(1-\nu)}[3(\boldsymbol{\eta}\cdot\mathbf{n})^2-1]. \quad (34)$$

There is a similarity between this equation and equations describing elastic interaction between two prismatic dislocation loops and between a prismatic dislocations loop and a dilatation center, for example a vacancy or a vacancy cluster. The first term in (34) is identical to Eq. (18) of Ref. [46], and its angular part is the same as that found by Foreman and Eshelby [48,49]. The second term in (34) is similar to Eq. (16) of Ref. [14]. The energy of elastic interaction between anisotropic defects (33) is strongly angularly dependent, and is maximum for the orientations where the vector $\mathbf{n}$ is parallel to $\boldsymbol{\eta}$.

TABLE IV. Dipole tensors of ⟨111⟩ dumbbell configurations in W computed using the Marinica EAM4 potential [44]. P_{ij} values are found using molecular statics assuming no relaxation of simulation cells. All the values are given in eV. Note the difference between P_{ij} values computed using empirical potentials and *ab initio* calculations. The predicted relaxation volumes of SIA defects vary from $\Omega_{\rm rel} = 1.235\Omega_0$ computed using a $4 \times 4 \times 4$ cell to $\Omega_{\rm rel} = 1.241\Omega_0$ computed using a $100 \times 100 \times 110$ cell. These values differ significantly from the relaxation volume of a SIA defect in tungsten $\Omega_{\rm rel} = 1.67\Omega_0$ predicted by DFT calculations [45].

Box size	P_{11}	P_{22}	P_{33}	P_{12}	P_{23}	P_{31}
$4 \times 4 \times 4$	36.99	36.99	36.99	17.35	17.35	17.35
$4 \times 4 \times 5$	37.76	37.76	37.18	17.33	16.96	16.96
$5 \times 5 \times 5$	38.71	38.71	38.71	18.26	18.26	18.26
$5 \times 5 \times 6$	37.80	37.80	37.85	17.10	16.91	16.91
$7 \times 7 \times 7$	37.54	37.54	37.54	16.68	16.68	16.68
$7 \times 7 \times 8$	37.48	37.48	37.51	16.66	16.61	16.61
$10 \times 10 \times 10$	37.32	37.32	37.32	16.58	16.58	16.58
$10 \times 10 \times 11$	37.30	37.30	37.31	16.58	16.57	16.57
$20 \times 20 \times 20$	37.19	37.19	37.19	16.58	16.58	16.58
$20 \times 20 \times 22$	37.19	37.19	37.19	16.59	16.58	16.58
$50 \times 50 \times 50$	37.17	37.17	37.17	16.59	16.59	16.59
$50 \times 50 \times 55$	37.17	37.17	37.17	16.59	16.59	16.59
$100 \times 100 \times 110$	37.16	37.16	37.16	16.59	16.59	16.59

VI. ELASTIC ENERGY OF A PERIODIC ARRAY OF DEFECTS

In applications, particularly in density functional theory calculations performed using periodic boundary conditions, it is desirable to evaluate the energy of elastic interaction between a defect structure situated in a simulation cell and the images of the same structure effectively periodically translated through space. If the original simulation cell is defined by the condition $\mathbf{r} \in V_{\rm cell}$, and the cell translation vectors are $\mathbf{R}_n = \mathbf{a}_1 n_1 + \mathbf{a}_2 n_2 + \mathbf{a}_3 n_3$, then the energy of elastic interaction between the defect structure in the original simulation cell and all its images equals [31]

$$E_{\rm int}^{\rm total} = \frac{1}{2} \sum_{n \neq 0} P_{ij} P_{kl} \frac{\partial}{\partial x_j} \frac{\partial}{\partial x_l} G_{ik}(\mathbf{R}_n). \qquad (35)$$

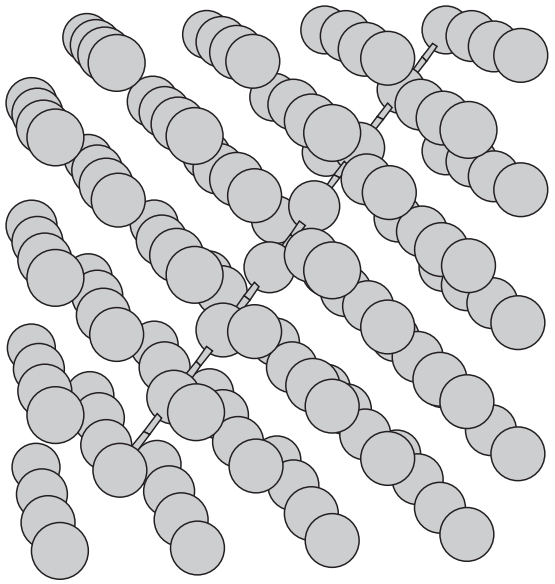

FIG. 2. Atomic structure of a self-interstitial atom defect in vanadium, where the orientation of the axis of the defect is close to the [111] direction. Atomic bonds are shown for the atoms that are significantly closer to each other than atoms in a perfect lattice, similarly to the case of tungsten illustrated in Fig. 1. Note that the strain field of a defect in vanadium is less localized than the strain field of tungsten.

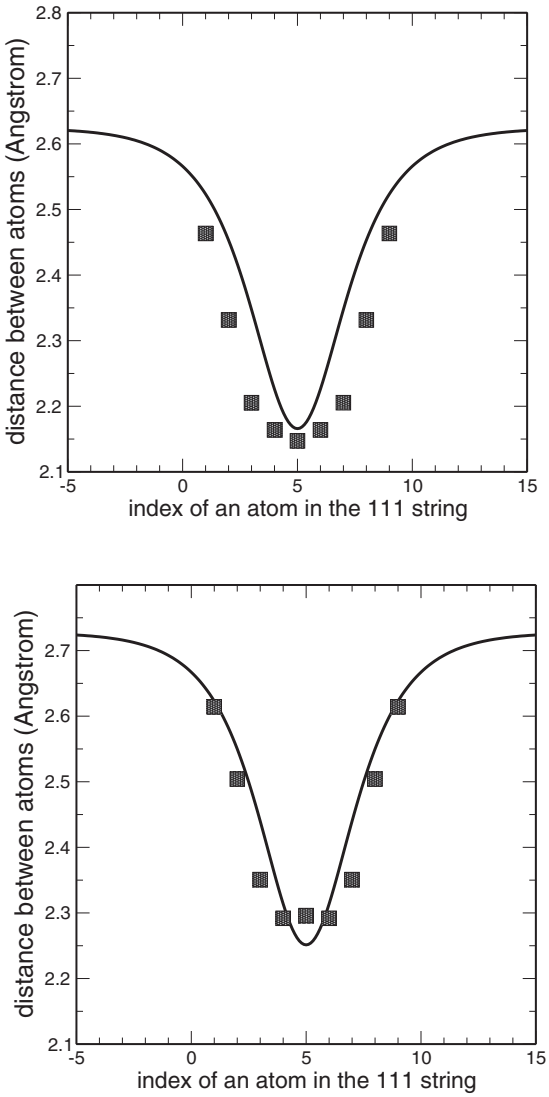

FIG. 3. Distances between atoms in the ⟨111⟩ most strongly distorted atomic strings in a simulation cell containing an SIA defect in vanadium (top) and tungsten (bottom). Continuous lines are solutions of the Frenkel-Kontorova model [47]; points are interatomic distances derived from DFT simulations. In agreement with the data given in Table IV, solutions of the Frenkel-Kontorova model show that to achieve convergence, atomistic calculations require simulation cells with linear dimensions approximately twice those of the cells typically used in DFT calculations.

For example, if we are interested in evaluating the elastic energy of interaction between a crowdion and its periodic images, we could use the analytical equation (33) and evaluate the above sum explicitly. However, a closer examination of the sum shows that this problem is not particularly well posed, as the sum (35) is only conditionally convergent. In other words, the result depends on the order of summation of the terms in the series [31,50]. This may appear as an unphysical oddity since the expression for the energy of interaction between two crowdions (33) is perfectly *bona fide* and can be used, for example, in dynamic simulations of Brownian motion of interacting defects [46].

The problem comes from the infinite number of defects in the material, interacting via long-range elastic forces, which in effect changes the very nature of the ground state of the system. This is evident from the fact that not only the energy of elastic interaction (35), but even the strain generated by the periodically translated images of a defect structure is effectively undefined. Indeed, the strain in the simulation cell produced by all the periodically translated images is

$$\epsilon_{ij}^{\text{images}}(\mathbf{r}) = -\sum_{n\neq 0} P_{kl}\frac{\partial}{\partial x_j}\frac{\partial}{\partial x_l}G_{ik}(\mathbf{r}-\mathbf{R}_n), \qquad (36)$$

where $\mathbf{r}\in V_{\text{cell}}$. Since at large distances $G_{ik}(\mathbf{r})\sim r^{-1}$, the total strain in the cell, given by Eq. (36), is a conditionally convergent quantity at any point $\mathbf{r}$ in the cell.

Naturally, this conditional convergence, or, in other words, the lack of a well-defined value of the sum (36), is not compatible with the requirement that under the condition of no overall relaxation of the simulation cell the total macroscopic strain should vanish,

$$\frac{1}{V_{\text{cell}}}\int_{V_{\text{cell}}}\left[\epsilon_{ij}^{(0)}(\mathbf{r})+\epsilon_{ij}^{\text{images}}(\mathbf{r})\right]dV = 0. \qquad (37)$$

Here $\epsilon_{ij}^{(0)}(\mathbf{r})$ is the strain associated with the defect structure situated in the cell itself. Under the condition of no relaxation of boundaries of the simulation cell, there is average nonvanishing stress in the cell, related to the dipole tensor through Eq. (28). Noting the relation between atomic displacements $\mathbf{u}(\mathbf{r})$ and the strain tensor $\epsilon_{ij}(\mathbf{r}) = (1/2)(\partial u_i/\partial x_j + \partial u_j/\partial x_i)$, we see that the above condition is consistent with the constraint that the field of atomic displacements is periodic, $\mathbf{u}(\mathbf{r}) = \mathbf{u}(\mathbf{r}+\mathbf{R}_n)\ \forall\ \mathbf{R}_n$. Hence enforcing condition (37) may help to solve the conditional convergence problem for the strain as well as for the energy of interaction between a defect and its periodic images [50].

To ensure that elastic strain generated by the images of defect structures associated with periodically translated cells satisfies condition (37), we subtract from strain given by (36) its spatially average value, defining the regularized strain generated by the periodic images in the simulation cell as

$$\epsilon_{ij}^{\text{images}}(\mathbf{r})\Big|_{\text{reg}} = \epsilon_{ij}^{\text{images}}(\mathbf{r}) - \frac{1}{V_{\text{cell}}}\int_{V_{\text{cell}}}\epsilon_{ij}^{\text{images}}(\mathbf{r})dV. \qquad (38)$$

Given that subtracting a constant term from the strain tensor is equivalent to subtracting a term that is linear in spatial coordinates from the field of atomic displacements, the above procedure is fully equivalent to the conditional summation regularization procedure proposed in Ref. [50]. When evaluating the total real strain in the cell, we should also replace $\epsilon_{ij}^{(0)}(\mathbf{r})$ in (37) by

$$\epsilon_{ij}^{(0)}(\mathbf{r}) - \frac{1}{V_{\text{cell}}}\int_{V_{\text{cell}}}\epsilon_{ij}^{(0)}(\mathbf{r})dV,$$

but since this renormalization has no effect on the conditional convergence of the sum (36), in what follows we are not going to discuss this point.

TABLE V. Equilibrium atomic volume $\Omega_0 = a_0^3/2$, parameters $\Omega^{(1)}$ and $\Omega^{(2)}$ of the elastic dipole tensor of a defect (18), the total elastic relaxation volume of the defect, and the same quantity expressed as a fraction of equilibrium atomic volume. All the dimensional values are given in cubic angstroms. The first row for each metal shows values computed using the zero strain method, while the second row gives values computed using the zero stress method. The elastic relaxation volume of a self-interstitial defect in tungsten given in the table agrees almost exactly with the value found earlier in Ref. [45].

	Ω_0	$\Omega^{(1)}$	$\Omega^{(2)}$	Ω_{rel}	$\Omega_{\text{rel}}/\Omega_0$
W	15.61	20.23	5.84	26.07	1.67
	15.61	20.48	5.55	26.02	1.67
Mo	15.61	17.38	5.29	22.67	1.45
	15.61	17.15	5.51	22.66	1.45
Ta	17.62	19.46	7.01	26.47	1.50
	17.62	17.77	8.46	26.23	1.49
Nb	17.68	30.46	-3.24	27.22	1.54
	17.68	20.57	6.18	26.75	1.51
V	12.91	−1.24	18.17	16.92	1.31
	12.91	−1.37	15.79	14.42	1.12

The energy of elastic interaction between a defect and its periodically translated images is linear in elastic strain. Hence, using (38), we find that the absolutely convergent expression for the energy of interaction between a defect and its periodic images is

$$E_{\text{int}} = \frac{1}{2}P_{ij}P_{kl}\sum_{n\neq 0}G_{ik,jl}(\mathbf{R}_n) - \frac{1}{2V_{\text{cell}}}P_{ij}P_{kl}\int_{V_{\text{cell}}}\sum_{n\neq 0}G_{ik,jl}(\mathbf{R}_n-\mathbf{r})dV. \qquad (39)$$

Both sums in the above expression are conditionally convergent as separate entities, but the sum of the two is convergent in the absolute sense if we perform the summation on a term-by-term basis. Indeed, by writing the above equation as

$$E_{\text{int}} = \frac{1}{2}P_{ij}P_{kl}\sum_{n\neq 0}\left[G_{ik,jl}(\mathbf{R}_n) - \frac{1}{V_{\text{cell}}}\int_{V_{\text{cell}}}G_{ik,jl}(\mathbf{R}_n-\mathbf{r})dV\right], \qquad (40)$$

we see that in the limit $|\mathbf{R}_n|\to\infty$, the difference between the two terms in square brackets is a quantity of order $O(R_n^{-4})$, ensuring the absolute convergence of the result.

Using values of parameters $\Omega^{(1)}$ and $\Omega^{(2)}$ taken from Table V, we have evaluated matrix elements of P_{ij} as functions

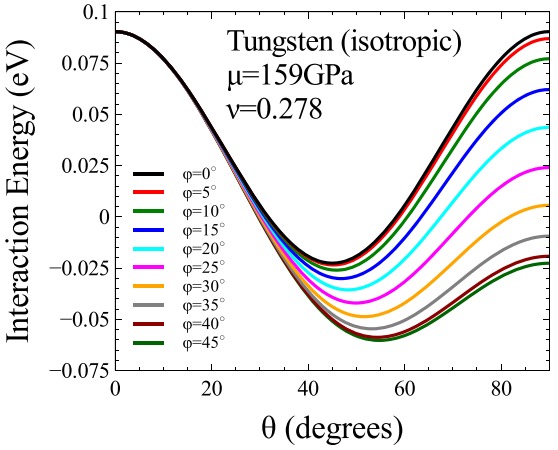

FIG. 4. Energy of elastic interaction between a SIA crowdion defect and its periodic images in tungsten as a function of the orientation of vector **n** computed in the isotropic elasticity approximation using data taken from Table V.

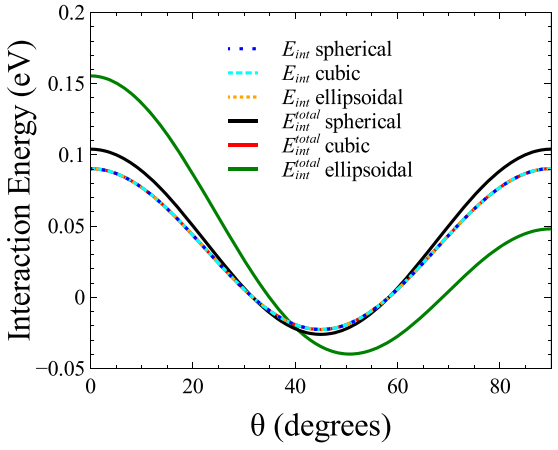

FIG. 5. Energy of elastic interaction between a SIA defect and its periodically translated images in tungsten in the plane $\phi = 0$. The curves were computed performing summation over (i) a sphere with radius 10 times the linear cell size, (ii) a cube with dimensions 30 times the linear cell size, and (iii) an ellipsoid where the three principal axes are 10, 15, and 20 times the linear cell size, respectively.

of the orientation of directional unit vector **n** of the defect. Figure 4 shows the energy of elastic interaction between an SIA defect and its periodic images in tungsten, computed using isotropic elasticity for a $4 \times 4 \times 4$ set of unit cells. The curve shown in the figure was computed assuming $\mu =$ 159 GPa and $\nu = 0.278$. Summation over the neighboring cells was performed within a sphere of radius ten times the linear dimension of a simulation cell. Elastic energy is minimum for the azimuthal angle $\phi = 45^\circ$ and the polar angle $\theta = 54.7356^\circ = \cos^{-1}(1/\sqrt{3})$, which correspond to the [111] crystallographic direction.

We have verified the convergence of $E_{\rm int}$ using various numerical implementations of the procedure for the evaluation of derivatives of the elastic Green's function [51]. Volume integration was performed using a nine-point Gaussian quadrature in each spatial dimension. Its convergence has been verified by comparing the results with calculations performed using an eleven-point Gaussian quadrature, and showing that the computed values do not change up to four significant figures. We have also checked the convergence of the sum by performing summation over a sphere of radius three times larger. Again, no change was found within four significant figures. In Fig. 5 we show that although $E_{\rm int}^{\rm total}$ is conditionally convergent, $E_{\rm int}$ is absolutely convergent and has the same value irrespective of how the terms in (40) are added numerically.

The figure illustrates the case of crowdions interacting in elastically isotopic tungsten, with the crowdion axis direction **n** lying in the plane $\phi = 0$. Sums (35) and (40) were evaluated using (i) summation over neighboring cells within a sphere of radius 10 times the linear cell size, (ii) summation over a cube with dimensions 30 times the linear cell size, and (iii) summation over an ellipsoid where the three principal axes are 10, 15, and 20 times the linear cell size, respectively. Values of $E_{\rm int}$ computed using all the above summation procedures remain the same. A curious point that we discovered when comparing the conditionally convergent and absolutely convergent expressions for the energy of elastic interaction between periodically translated defects is that the correction term in Eq. (40) can be effectively ignored if the summation is performed using cubes of gradually increasing size.

We have also computed the energy of elastic interaction $E_{\rm int}$ between a defect and its periodically translated images in the anisotropic elasticity approximation, using Eq. (40) and evaluating the second derivatives of the elastic Green's function numerically [51]. In all the bcc transition metals, the most elastically stable configuration of a SIA defect, computed assuming periodically translated cubic simulation cells, corresponds to the ⟨111⟩ orientation of the axis of the defect; see Fig. 6. This finding can be explained by noting that in a simple cubic lattice of defects, the closest nearest neighbors are situated at $(\pm L,0,0)$, $(0,\pm L,0)$, and $(0,0,\pm L)$, where L is the dimension of the simulation cell. Equation (34) suggests that the elastic energy should be maximum when the direction of the axis of the defect is close to a ⟨001⟩ direction, in agreement with the data shown in Fig. 6.

Concluding this section, we note that while the variation of the total elastic energy as a function of the orientation of crowdion defects computed above for a periodic arrangement of defects agrees with results derived using the computer program given in Ref. [31], the absolute values of elastic energy per defect computed using the two numerical procedures, i.e., the one outlined above and the one developed in Ref. [31], differ. The difference amounts to a constant factor, and it does not affect the conclusion about the ⟨111⟩ crowdion defect representing the lowest elastic energy configuration, both in isotropic and anisotropic elasticity approximations.

VII. SUMMARY AND CONCLUSIONS

We have derived analytical formulas for the matrix elements of elastic dipole tensors of self-interstitial atom defects, using isotropic and anisotropic elasticity approximations. The equations show that, in addition to the prismatic dislocation looplike character, the elastic field of a SIA defect has a significant isotropic dilatation component. Using DFT calculations, we

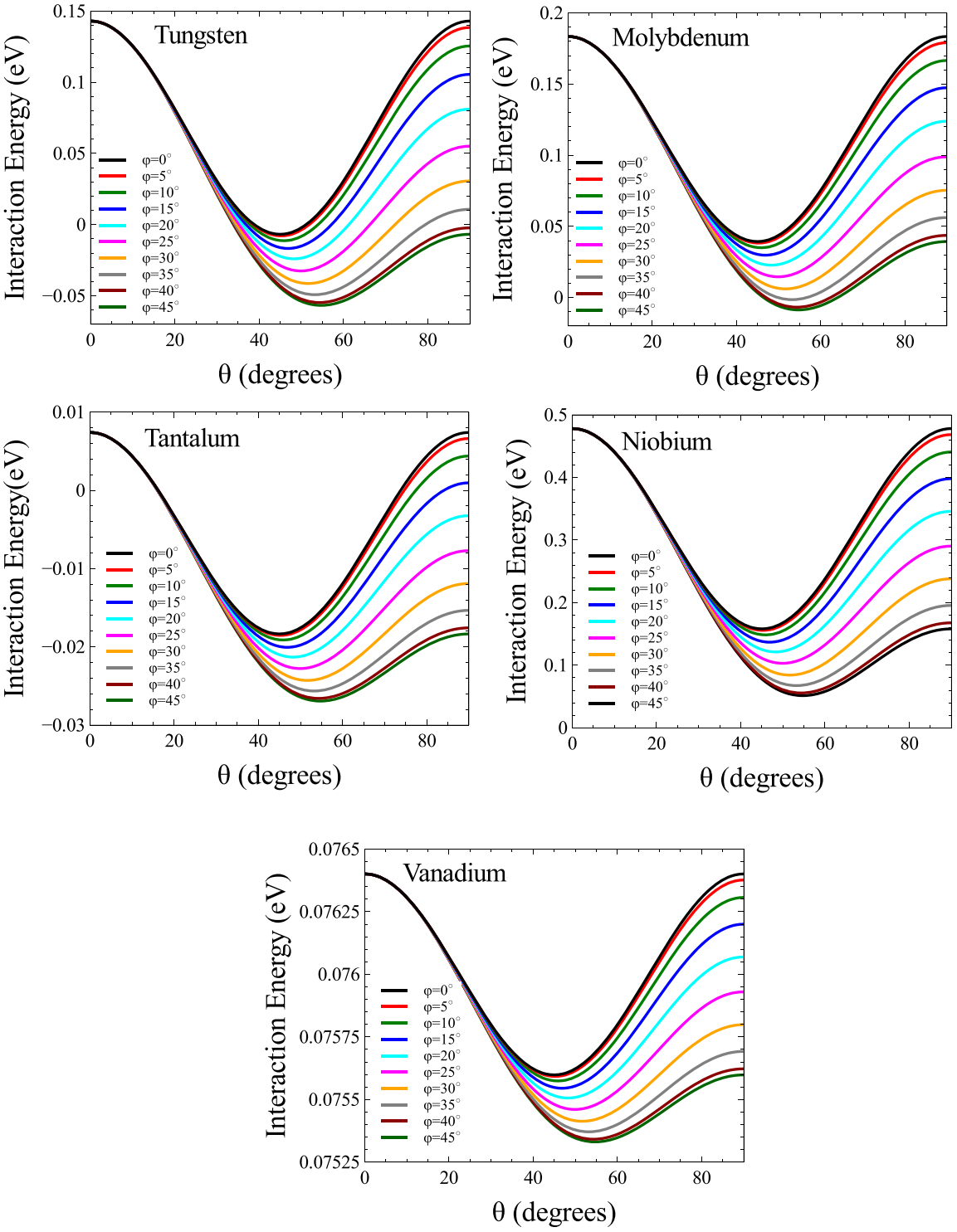

FIG. 6. The energy of elastic interaction between a ⟨111⟩ SIA defect and its periodic images as a function of the orientation of vector **n**, computed in the full anisotropic elasticity approximation for tungsten, molybdenum, tantalum, niobium, and vanadium.

have parametrized dipole tensors of ⟨111⟩ defects for all the nonmagnetic bcc transition metals. We then used the data to evaluate the energy of elastic interaction between defects, and we found that in a periodic three-dimensional arrangement of defects, long-range elastic interactions favor the ⟨111⟩ orientation of their axes, an effect resulting from the interaction between a defect and all its images in a simulation involving periodic boundary conditions.

ACKNOWLEDGMENTS

This work has been carried out within the framework of the EUROfusion Consortium and has received funding from the Euratom research and training programme 2014-2018 under Grant Agreements No. 633053 and No. 755039. Also, it has been partially funded by the RCUK Energy Programme (Grant No. EP/P012450/1). The views and opinions expressed herein

do not necessarily reflect those of the European Commission. We also acknowledge EUROfusion for the provision of access to Marconi supercomputer facility at CINECA, Bologna, Italy. To obtain further information on the data and models underlying this paper, please contact PublicationsManager@ukaea.uk.

We are grateful to C.-H. Woo and A.P. Sutton for the discussions that stimulated this study, and to M.-C. Marinica for bringing to our attention the issue of conditional convergence of elastic energy in a periodic system of interacting defects.

[1] A. R. Allnatt, *Crystal Lattice Defects and Matter Transport, in Selected Topics in Physics, Astrophysics, and Biophysics*, edited by E. A. de Loredo and N. K. Jurisic, in *Proceedings of the XIV Latin American School of Physics, 1972* (Kluwer Academic, Dordrecht, 1973), Vol. 3-43, pp. 3–42.

[2] S. Han, L. A. Zepeda-Ruiz, G. J. Ackland, R. Car, and D. J. Srolovitz, Self-interstitials in V and Mo, Phys. Rev. B **66**, 220101 (2002).

[3] D. Nguyen-Manh, A. P. Horsfield, and S. L. Dudarev, Self-interstitial atom defects in bcc transition metals: Group-specific trends, Phys. Rev. B **73**, 020101 (2006).

[4] P. M. Derlet, D. Nguyen-Manh, and S. L. Dudarev, Multiscale modeling of crowdion and vacancy defects in body-centered-cubic transition metals, Phys. Rev. B **76**, 054107 (2007).

[5] S. L. Dudarev, Density functional theory models for radiation damage, Annu. Rev. Mater. Res. **43**, 35 (2013).

[6] A. E. Sand, K. Nordlund, and S. L. Dudarev, Radiation damage production in massive cascades initiated by fusion neutrons in tungsten, J. Nucl. Mater. **455**, 207 (2014).

[7] A. E. Sand, M. J. Aliaga, M. J. Caturla, and K. Nordlund, Surface effects and statistical laws of defects in primary radiation damage: Tungsten versus iron, Europhys. Lett. **115**, 36001 (2016).

[8] M. W. Thompson, The damage and recovery of neutron irradiated tungsten, Philos. Mag. **5**, 278 (1960).

[9] F. Dausinger and H. Schultz, Long-Range Migration of Self-Interstitial Atoms in Tungsten, Phys. Rev. Lett. **35**, 1773 (1975).

[10] T. D. Swinburne, P.-W. Ma, and S. L. Dudarev, Low temperature diffusivity of self-interstitial defects in tungsten, New J. Phys. **19**, 073024 (2017).

[11] S. L. Dudarev, The non-Arrhenius migration of interstitial defects in bcc transition metals, C. R. Phys. **9**, 409 (2008).

[12] T. D. Swinburne, S. L. Dudarev, and A. P. Sutton, Classical Mobility of Highly Mobile Crystal Defects, Phys. Rev. Lett. **113**, 215501 (2014).

[13] T. D. Swinburne and S. L. Dudarev, Phonon drag force acting on a mobile crystal defect: Full treatment of discreteness and nonlinearity, Phys. Rev. B **92**, 134302 (2015).

[14] S. L. Dudarev and A. P. Sutton, Elastic interactions between nano-scale defects in irradiated materials, Acta Mater. **125**, 425 (2017).

[15] J. P. Hirth and J. Lothe, *Theory of Dislocations* (Krieger, Malabar, 1992).

[16] J. Marian, B. D. Wirth, J. M. Perlado, G. R. Odette, and T. Diaz de la Rubia, Dynamics of self-interstitial migration in Fe-Cu alloys, Phys. Rev. B **64**, 094303 (2001).

[17] Z. Chen, N. Kioussis, N. Ghoniem, and D. Seif, Strain-field effects on the formation and migration energies of self interstitials in α-Fe from first principles, Phys. Rev. B **81**, 094102 (2010).

[18] G. Leibfried and N. Breuer, *Point Defects in Metals* (Springer, Berlin, 1978), pp. 145–164.

[19] A. B. Sivak, P. A. Sivak, V. A. Romanov, and V. M. Chernov, Energetic, crystallographic and diffusion characteristics of hydrogen isotopes in iron, J. Nucl. Mater. **461**, 308 (2015).

[20] A. B. Sivak, P. A. Sivak, V. A. Romanov, and V. M. Chernov, Hydrogen diffusion in the elastic fields of dislocations in iron, Phys. At. Nucl. **79**, 1199 (2016).

[21] T. Mura, *Micromechanics of Defects in Solids* (Kluwer, Dordrecht, 1991), p. 22.

[22] H. Trinkaus, On the investigation of small dislocation loops in cubic crystals by diffuse X-ray scattering, Phys. Status Solidi B **54**, 209 (1972).

[23] P. H. Dederichs, C. Lehmann, H. R. Schober, A. Scholz, and R. Zeller, Lattice theory of point defects, J. Nucl. Mater. **69**, 176 (1978).

[24] L. D. Landau and E. M. Lifshits, *Theory of Elasticity*, 3rd ed. (Butterworth-Heinemann, Oxford, 1986), p. 112.

[25] J. F. Nye, *Physical Properties of Crystals* (Oxford University Press, Oxford, UK, 1985).

[26] T. D. Swinburne, K. Arakawa, H. Mori, H. Yasuda, M. Isshiki, K. Mimura, M. Uchikoshi, and S. L. Dudarev, Fast, vacancy-free climb of prismatic dislocation loops in bcc metals, Sci. Rep. **6**, 30596 (2016).

[27] Y. N. Osetsky, D. J. Bacon, A. Serra, B. N. Singh, and S. I. Golubov, One-dimensional atomic transport by clusters of self-interstitial atoms in iron and copper, Philos. Mag. **83**, 61 (2003).

[28] P. M. Derlet, M. R. Gilbert, and S. L. Dudarev, Simulating dislocation loop internal dynamics and collective diffusion using stochastic differential equations, Phys. Rev. B **84**, 134109 (2011).

[29] I. Rovelli, S. L. Dudarev, and A. P. Sutton, Non-local model for diffusion-mediated dislocation climb and cavity growth, J. Mech. Phys. Solids **103**, 121 (2017).

[30] E. Clouet, S. Garruchet, H. Nguyen, M. Perez, and C. S. Becquart, Dislocation interaction with C in α-Fe: A comparison between atomic simulations and elasticity theory, Acta Mater. **56**, 3450 (2008).

[31] C. Varvenne, F. Bruneval, M.-C. Marinica, and E. Clouet, Point defect modeling in materials: Coupling *ab initio* and elasticity approaches, Phys. Rev. B **88**, 134102 (2013).

[32] R. C. Pasianot, On the determination of defect dipoles from atomistic simulations using periodic boundary conditions, Philos. Mag. Lett. **96**, 447 (2016).

[33] R. Nazarov, J. S. Majevadia, M. Patel, M. R. Wenman, D. S. Balint, J. Neugebauer, and A. P. Sutton, First-principles calculation of the elastic dipole tensor of a point defect: Application to hydrogen in α-zirconium, Phys. Rev. B **94**, 241112 (2016).

[34] C. Varvenne and E. Clouet, Elastic dipoles of point defects from atomistic simulations, Phys. Rev. B **96**, 224103 (2017).

[35] G. Kresse and J. Hafner, *Ab initio* molecular dynamics for liquid metals, Phys. Rev. B **47**, 558 (1993).

[36] G. Kresse and J. Hafner, *Ab initio* molecular-dynamics simulation of the liquid-metal-amorphous-semiconductor transition in germanium, Phys. Rev. B **49**, 14251 (1994).

[37] G. Kresse and J. Furthmüller, Efficiency of *ab-initio* total energy calculations for metals and semiconductors using a plane-wave basis set, Comput. Mater. Sci. **6**, 15 (1996).

[38] G. Kresse and J. Furthmüller, Efficient iterative schemes for *ab initio* total-energy calculations using a plane-wave basis set, Phys. Rev. B **54**, 11169 (1996).

[39] R. Armiento and A. E. Mattsson, Functional designed to include surface effects in self-consistent density functional theory, Phys. Rev. B **72**, 085108 (2005).

[40] A. E. Mattsson and R. Armiento, Implementing and testing the AM05 spin density functional, Phys. Rev. B **79**, 155101 (2009).

[41] A. E. Mattsson, R. Armiento R, J. Paier, G. Kresse, J. M. Wills, and T. R. Mattsson, The AM05 density functional applied to solids, J. Chem. Phys **128**, 084714 (2008).

[42] Y. Le Page and P. Saxe, Symmetry-general least-squares extraction of elastic data for strained materials from *ab initio* calculations of stress, Phys. Rev. B **65**, 104104 (2002).

[43] S. Plimpton, Fast parallel algorithms for short-range molecular dynamics, J. Comput. Phys. **117**, 1 (1995).

[44] M.-C. Marinica, L. Ventelon, M. R. Gilbert, L. Proville, S. L. Dudarev, J. Marian, G. Bencteux, and F. Willaime, Interatomic potentials for modeling radiation defects and dislocations in tungsten, J. Phys.: Condens. Matter **25**, 395502 (2013).

[45] F. Hofmann, D. Nguyen-Manh, M. R. Gilbert, C. E. Beck, J. K. Eliason, A. A. Maznev, W. Liu, D. E. J. Armstrong, K. A. Nelson, and S. L. Dudarev, Lattice swelling and modulus change in a helium-implanted tungsten alloy: X-ray micro-diffraction, surface acoustic wave measurements, and multiscale modelling, Acta Mater. **89**, 352 (2015).

[46] S. L. Dudarev, M. R. Gilbert, K. Arakawa, H. Mori, Z. Yao, M. L. Jenkins, and P. M. Derlet, Langevin model for real-time Brownian dynamics of interacting nanodefects in irradiated metals, Phys. Rev. B **81**, 224107 (2010); S. L. Dudarev, K. Arakawa, X. Yi, Z. Yao, M. L. Jenkins, M. R. Gilbert, and P. M. Derlet, Spatial ordering of nano-dislocation loops in ion-irradiated materials, J. Nucl. Mater. **455**, 16 (2014).

[47] S. L. Dudarev, Coherent motion of interstitial defects in a crystalline material, Philos. Mag. **83**, 3577 (2003).

[48] A. J. E. Foreman and J. D. Eshelby, *Elastic Interaction Energy of Dislocation Loops*, Report AERE-R4170 (Atomic Energy Research Establishment, Harwell, UK, 1962).

[49] R. S. Barnes, The migration of large clusters of point defects in irradiated materials, J. Phys. Soc. Jpn. **18**, Supplement III, 305 (1963).

[50] W. Cai, V. V. Bulatov, J. Chang, J. Li, and S. Yip, Periodic image effects in dislocation modelling, Philos. Mag. **83**, 539 (2003).

[51] D. M. Barnett, The precise evaluation of derivatives of the anisotropic elastic Green's functions, Phys. Status Solidi B **49**, 741 (1972).